

# Nanometal Dust Explosion in Confined Vessel: Combustion and Kinetic Analysis

Khairiah Mohd Mokhtar, Rafiziana Md Kasmani,\* Che Rosmani Che Hassan, Mahar Diana Hamid, Mohamad Iskandr Mohamad Nor, Mohd Usman Mohd Junaidi, and Norazana Ibrahim



Cite This: *ACS Omega* 2021, 6, 17831–17838



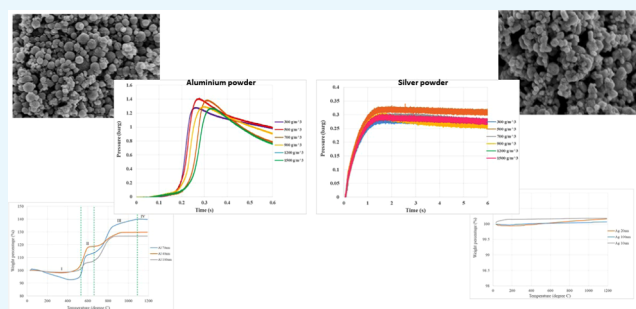
Read Online

ACCESS |

Metrics & More

Article Recommendations

**ABSTRACT:** Extensive application of metal powder, particularly in nanosize could potentially lead to catastrophic dust explosion, due to their pyrophoric behavior, ignition sensitivity, and explosivity. To assess the appropriate measures preventing accidental metal dust explosions, it is vital to understand the physicochemical properties of the metal dust and their kinetic mechanism. In this work, explosion severity of aluminum and silver powder, which can be encountered in a passivated emitter and rear contact (PERC) solar cell, was explored in a 0.0012 m<sup>3</sup> cylindrical vessel, by varying the particle size and powder concentration. The  $P_{\max}$  and  $dP/dt_{\max}$  values of metal powder were demonstrated to increase with decreasing particle size. Additionally, it was found that the explosion severity of silver powder was lower than that of aluminum powder due to the more apparent agglomeration effect of silver particles. The reduction on the specific surface area attributed to the particles' agglomeration affects the oxidation reaction of the metal powder, as illustrated in the thermogravimetric (TG) curves. A sluggish oxidation reaction was demonstrated in the TG curve of silver powder, which is contradicted with aluminum powder. From the X-ray photoelectron spectroscopy (XPS) analysis, it is inferred that silver powder exhibited two reactions in which the dominant reaction produced Ag and the other reaction formed Ag<sub>2</sub>O. Meanwhile, for aluminum powder, explosion products only comprise Al<sub>2</sub>O<sub>3</sub>.



## 1. INTRODUCTION

Applications of metals are in demand for automotive, electronics, aerospace, and 3D-printing industries due to their high mechanical strength, thermal resistivity, electrical conductivity, and excellent corrosion resistance properties. Metals are widely used as the composition of plastics, paints, inks, rubber, fibers, detergents, and even drugs.<sup>1</sup> However, wider use of metal powder could potentially lead to catastrophic dust explosion, which would cause fatality and properties destruction, due to its pyrophoric behavior, ignition sensitivity, and explosivity, which should be taken into consideration when they are in nanoscale sizes. To take appropriate measures to prevent accidental metal dust explosions, it is necessary to sufficiently understand the mechanism of metal dust explosion, physicochemical properties, and the kinetic mechanism in this medium. Nanomaterials have emerged in recent years, corresponding to the advanced development of nanotechnology industries, and hence, it is essential to take into account the influence of nanosize particles on the ignition sensitivity and explosivity of the metal powder to give some fundamental principles on nanometal dust risk assessment particularly when more than two metals are involved in a mixture.

To the best of the authors' knowledge, there is a scarcity of data on the explosion behaviors when metal mixtures are in context. In a study conducted on iron nanoparticles and carbon nanofibers, it was found that the lower heat dissipation and pyrophoric properties of the metal nanoparticles triggered an ignition of carbon nanofiber and facilitated the propagation of combustion.<sup>2</sup> Meanwhile, another study demonstrated that pure aluminum powder has higher explosion pressure due to its high oxidation kinetics, indicating higher explosion risk than aluminum–silicon mixture.<sup>3</sup> Additionally, it is noteworthy that the explosion severity of mixtures may be enhanced due to hydrogen production from the reaction of metals with water vapor at high temperatures.<sup>4</sup> These findings suggest that one should not assume that the explosion severity of mixtures normally corresponds with the dominant element properties, but it can be deduced to many factors. This condition leads to

Received: February 22, 2021

Accepted: June 30, 2021

Published: July 10, 2021



many unanswered assumptions on nanoparticles explosion in mixtures, particularly when both metals are from different functional groups. The explosion severity of mixtures may be higher than that of the pure powder due to the enhanced oxidation reaction contributed by metal powder, or vice versa. Further, studies on nanometal dust particles show that the complexity of the physicochemical properties and the kinetic chemical mechanism can be questioned when two or more metal dust are mixed. On the other hand, the agglomeration effects caused by different levels of attraction forces between particles must result in different physicochemical behaviors in dust explosion. Therefore, to give insight into the fundamental principles of dust explosion when dust is in a mixture form, this work will be solely focused on the investigation of the combustion kinetic mechanism in relation to the explosion severity of two metal powders from different functional groups, namely, aluminum and silver, which can be encountered in a passivated emitter and rear contact (PERC) solar cell. The second part will discuss, in detail, about the effect of silver inhibition on aluminum dust explosion that will be published later.

## 2. METHODS

**2.1. Materials.** Aluminum powder comprising three particle sizes (i.e., 40, 70, and 100 nm) was supplied by Hongwu International Group Ltd., China. Meanwhile, three particle sizes of silver powder (i.e., 20 nm, 100 nm, and Ag 10  $\mu\text{m}$ ) were purchased from GetNanoMaterials, Oocap Inc., France. Both sample powders were stored in a desiccator to prevent exposure to moisture that might affect the experimental results. The specific surface area of all sizes of aluminum and silver powder was identified using the Brunauer–Emmett–Teller (BET) method. The results are tabulated in Table 1.

**Table 1. Specific Surface Area of Aluminum and Silver Particles**

chemical formula	aluminum			silver		
	Al			Ag		
average particle size	40 nm	70 nm	100 nm	20 nm	100 nm	10 $\mu\text{m}$
BET surface area ( $\text{m}^2/\text{g}$ )	32.15	53.41	24.36	9.36	7.89	0.26

**2.2. Samples' Characterizations.** Field emission scanning electron microscopy (FESEM), thermogravimetric analysis (TGA), and X-ray photoelectron spectroscopy (XPS) were conducted to identify the morphological structure, oxidation reaction, and chemical compositions of the metal powder, respectively. The oxidation reactions of the metal powder were investigated by TGA in an air environment with a flow rate of 10 L/min and a heating rate of 10  $^{\circ}\text{C}/\text{min}$ . Meanwhile, XPS was conducted at an anode voltage of 15 kV and a power level of 300 W. The pass energy was 100 eV for survey spectra and 50 eV for high-resolution spectra. The spectra were curve-fitted using the CasaXPS software. Original spectra were calibrated by the reference energy of C1s signal at a binding energy of 284.6 eV and smoothed.

**2.3. Experimental Apparatus and Methods.** Dust explosion experiments were performed in a 0.0012  $\text{m}^3$  stainless steel cylindrical test vessel with an internal diameter of 70 mm and a height of 304 mm. The experimental setup is shown

schematically in Figure 1. The metal powder was placed in the dispersion cup, and the test vessel was tightened up. The

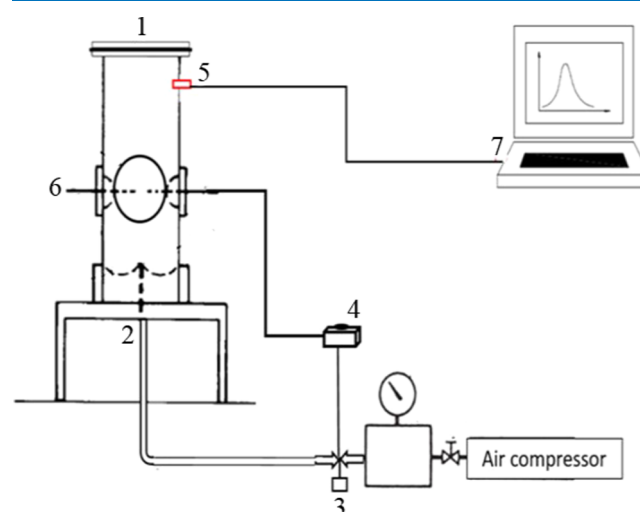


**Figure 1.** Experimental apparatus. 1. Test vessel, 2. Gas nozzle, 3. Solenoid valve, 4. Time controller, 5. Pressure transducer, 6. Igniter, 7. Data acquisition system.

sample was dispersed by compressed air at a pressure of 6 bar. After the dispersion, the sample was ignited by a centrally mounted igniter, following a 60 ms time delay. The powder concentration varied from 300 to 1500  $\text{g}/\text{m}^3$ . Each test of both aluminum and silver explosion was performed in at least three replications for accuracy and reproducibility. The explosion pressure evolutions were measured by a piezoelectric pressure transducer (Keller Series 11, accuracy:  $\pm 0.001$  s) and recorded by a data acquisition system from National Instruments with a sampling rate of 100 MHz. These data yielded maximum explosion pressure ( $P_{\text{max}}$ ) from the pressure–time profiles. Meanwhile, the maximum rate of pressure rise ( $dP/dt_{\text{max}}$ ) was calculated based on the tangent of the pressure–time profiles.

## 3. RESULTS AND DISCUSSION

**3.1. Explosion Characteristics of Single Metal Powder in a Confined Vessel.** The pressure–time histories of different particle sizes of both aluminum and silver powders in various powder concentrations are shown in Figure 2a–f. The experimental standard deviation in the maximum explosion pressure ( $P_{\text{max}}$ ) and  $dP/dt_{\text{max}}$  (i.e., tangent of the graph) values of each metal powder at different concentrations was in the range of 0.001–0.005, implying that the data spread was closer to the mean values and repetitive. All graphs in Figure 2a–c display similar pressure–time profiles with different maximum explosion pressure as a function of powder concentration. It should be noted that 300  $\text{g}/\text{m}^3$  is the minimum explosible concentration (MEC) for both metal powder. Meanwhile, the optimum explosion concentration for all sizes of aluminum and silver powder is 500  $\text{g}/\text{m}^3$ . As presented in Figure 2, it can be observed that the explosion pressure increased with powder concentration at poor dust/air mixtures until powder concentration up to 500  $\text{g}/\text{m}^3$ , before decreasing at powder concentrations of 700 and 900  $\text{g}/\text{m}^3$ . Meanwhile, stable values can be seen at concentrations of 1200 and 1500  $\text{g}/\text{m}^3$ . For instance, the corresponding  $P_{\text{max}}$  of Al 40 nm to the powder concentration of 300  $\text{g}/\text{m}^3$  is 1.324 barg. When the powder concentration was 500  $\text{g}/\text{m}^3$ ,  $P_{\text{max}}$  reached

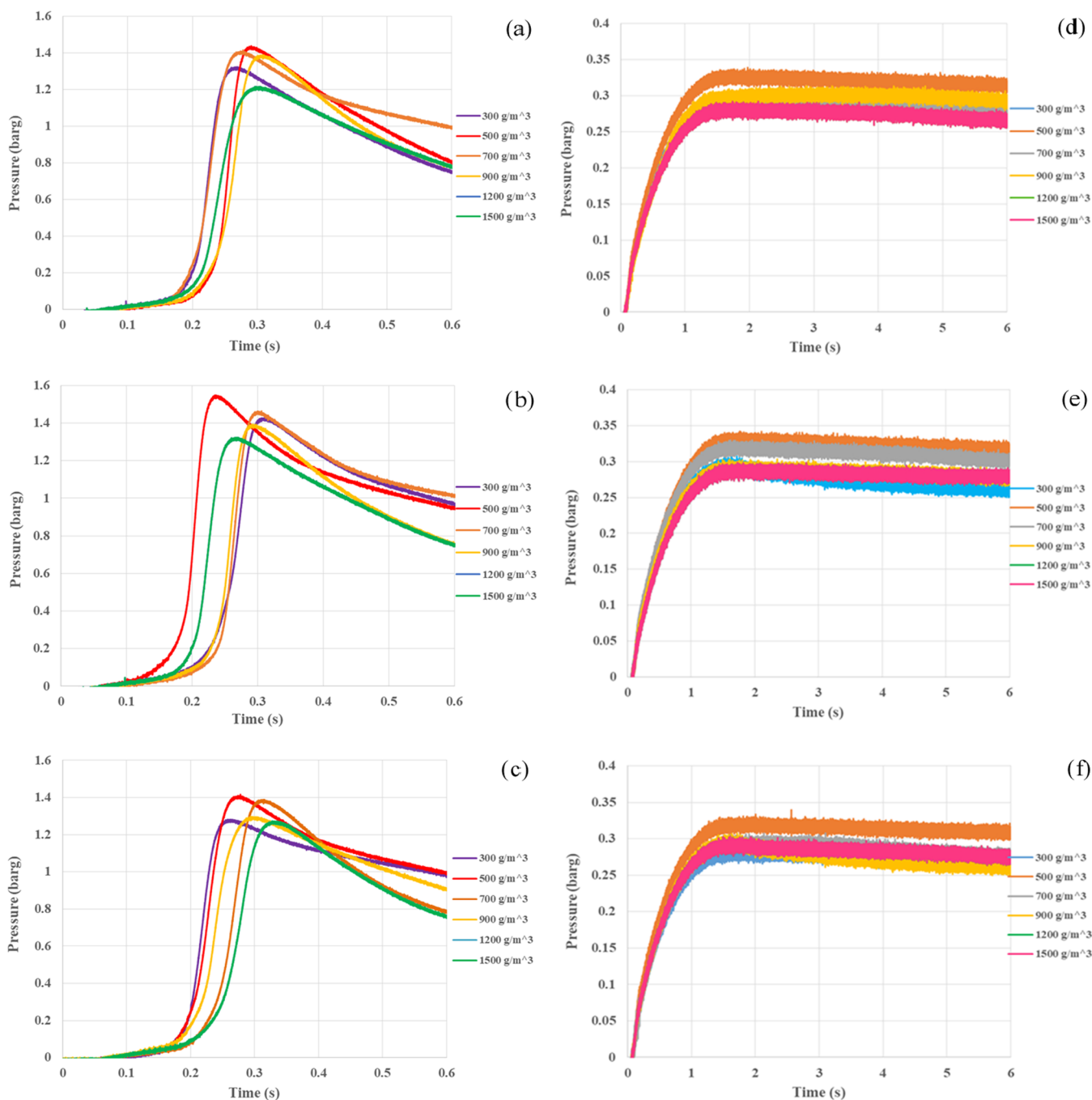


**Figure 2.** Explosion pressure–time histories of (a) Al 40 nm, (b) Al 70 nm, (c) Al 100 nm, (d) Ag 20 nm, (e) Ag 10  $\mu\text{m}$ , and (f) Ag 100 nm at various powder concentrations.

the maximum value of 1.438 barg. Then,  $P_{\text{max}}$  decreases from 1.416 to 1.389 barg at 700 and 900  $\text{g}/\text{m}^3$ , respectively. A similar trend is also demonstrated in silver powder explosion as presented in Figure 2d–f. The  $P_{\text{max}}$  value of Ag 20 nm increases from 0.296 to 0.334 barg when the silver powder concentration increases from 300 to 500  $\text{g}/\text{m}^3$ , before reducing at 700 and 900  $\text{g}/\text{m}^3$ , and reaching constant  $P_{\text{max}}$  values with a further increase in the concentration (as indicated by the overlapping pressure–time profiles). These results are due to the fact that, at very high powder concentrations (700–1500  $\text{g}/\text{m}^3$ ), in the rich-fuel limit, the shortened interparticle distance attributed to the large number of particles per unit volume and oxygen deficiency results in the reduction of the

heat transfer rate and subsequently its explosion severity. These results are in good agreement with other investigation elsewhere.<sup>5–7</sup>

**3.2. Influence of Metal Particle Size on  $P_{\text{max}}$  and  $dP/dt_{\text{max}}$ .** For the effect of the metal particle size on dust explosion, it is found that the  $P_{\text{max}}$  and  $dP/dt_{\text{max}}$  values of Al 40 nm are lower than those of Al 70 nm at similar powder concentrations. As can be seen in Figure 2a,b, at a 500  $\text{g}/\text{m}^3$  powder concentration, the  $P_{\text{max}}$  value of Al 70 nm is 1.549 barg, 7.2% higher than that of Al 40 nm. Meanwhile, the  $dP/dt_{\text{max}}$  of Al 40 nm is 28.721 barg/s compared to 31.567 barg/s of Al 70 nm.

A decrease in particle size would enhance a particle's specific surface area, which gives a larger surface area for oxidation, accelerating the particles' burning rate and the overall kinetics of the explosion reaction, hence increasing the  $P_{\max}$  value.<sup>8–10</sup> As presented in Figure 3, when the specific surface area of the

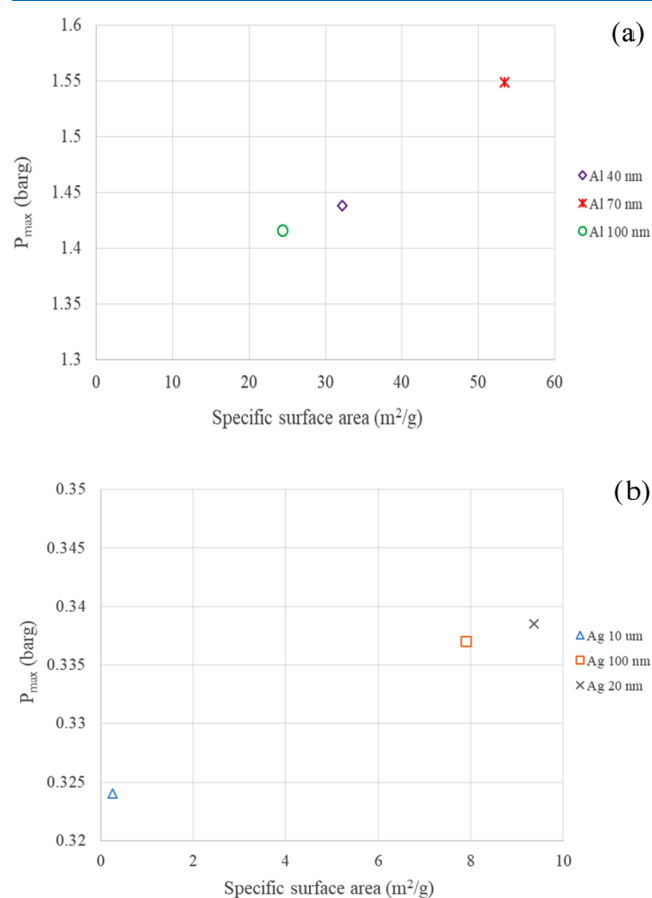


**Figure 3.** Effect of specific surface area on  $P_{\max}$  values of (a) aluminum powder and (b) silver powder.

metal powder increases, the  $P_{\max}$  value increases. For instance, increasing the specific surface area of silver powder from 7.89  $\text{m}^2/\text{g}$  (Ag 100 nm) to 9.36  $\text{m}^2/\text{g}$  (Ag 20 nm) resulted in a corresponding increase in the  $P_{\max}$  values from 0.332 to 0.337 barg. Similarly, the higher  $P_{\max}$  value of Al 70 nm corresponded to the larger specific surface area of Al 70 nm (53.41  $\text{m}^2/\text{g}$ ) compared to Al 100 nm (24.36  $\text{m}^2/\text{g}$ ). The higher  $P_{\max}$  values of Al 70 nm and Ag 20 nm were attributed to accelerated explosion reaction kinetics, which cause the metal particles to be oxidized easily, hence shortening the time to reach  $P_{\max}$  as illustrated in Figure 2. The changes in the  $P_{\max}$  and  $dP/dt_{\max}$  values subsequently lead to lower explosion severity index,  $K_{st}$  ( $K_{st} = (dP/dt_{\max})V^{1/3}$ ), values of Al 70 nm and Ag 20 nm compared to Al 100 nm and Ag 100 nm, respectively (see Figure 4).

However, it is noteworthy that the specific surface area of silver powder is much smaller than aluminum powder (see Figure 3b). Since nanoscale is prone to agglomeration effect, the pre- and postexplosion morphological structures were carried out using FESEM analysis. The agglomeration effect on the silver powder is more pronounced compared to that of the aluminum powder (as demonstrated in Tables 2 and 3), implying that the mass burning rate is significantly reduced due

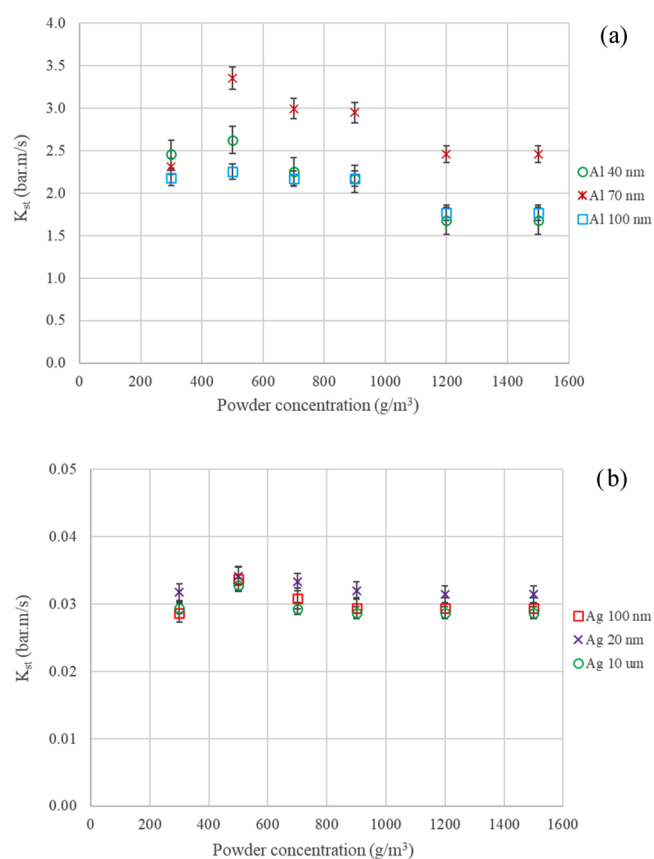


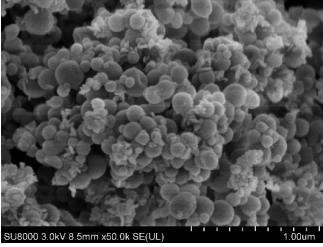
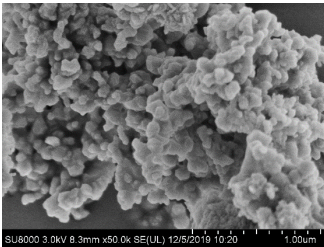
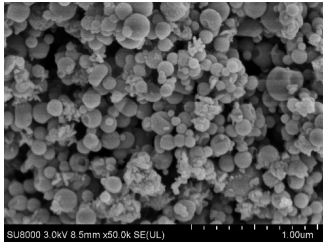
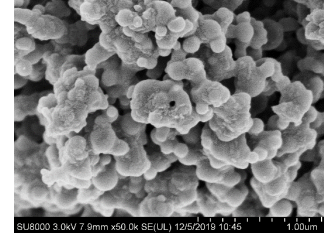
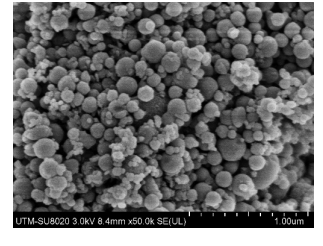
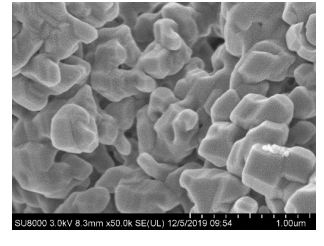
**Figure 4.** Explosion severity index ( $K_{st}$ ) of (a) aluminum powder and (b) silver powder.

to the smaller specific area, hence justifying the lower  $P_{\max}$  and  $K_{st}$  values. It also should be noted that for postexplosion, the agglomeration effect of silver particles becomes more significant, as can be clearly seen in Table 3 on the Ag 20 nm particle structure. Meanwhile, the irregular spliced structures were demonstrated in the aluminum explosion product. These morphological structures of aluminum powder are consistent with the literature,<sup>11,12</sup> which reported that the aluminum morphology is formed as a result of the condensation of gas-phase reaction. The agglomeration effect, which tends to occur in nanodusts, is attributed to the insufficient aerodynamic forces to obstruct the interparticle attraction and subsequently inhibits the dispersion of particles into a primary particle cloud.<sup>13,14</sup>

**3.3. Oxidation Reaction of Metal Powder.** Thermogravimetric (TG) analysis was conducted to investigate the oxidation reaction of the metal powder. Referring to Figure 5, the trend of aluminum TG curves is similar to the literature,<sup>15</sup> in which the oxidation reaction of aluminum particles is divided into four stages. In the temperature range of 27–520  $^{\circ}\text{C}$ , a substantial weight decreases in stage I is due to the loss of moisture. Meanwhile, a noticeable weight increase up to the temperature of 650  $^{\circ}\text{C}$  can be observed in stage II, which is the surface oxidation stage, prior to stage III, which is referred to as the melt and broken stage. The last stage, i.e., stage IV, is the burning stage.

It can be observed in Figures 5 and 6 that the oxidation reaction of aluminum and silver, respectively, which was indicated by particle weight gaining, was affected by the agglomeration of particles. The reduction of the specific

Table 2. Morphological Structures of Various Sizes of Aluminum Powder

	Pre-explosion	Post-explosion
Al 40 nm		
Al 70 nm		
Al 100 nm		

surface area of particles attributed to the agglomeration effect causes a slower oxidation reaction of the metal powder and hence reduces the particle weight gain. It can be observed in Figure 5 that the proportion of particle weight gaining in stage II increases with decreasing aluminum particle size. This result showed a reasonable agreement with the literature<sup>15</sup> that the proportion of particle weight gain corresponding to the particle oxidation reaction would be reduced significantly with increasing aluminum particle size. When the particle size becomes smaller, the proportion of particle weight gain would increase due to the larger specific surface area for oxidation. A closer look should be focused on the oxidation reaction of Al 70 nm and Al 100 nm. The change in the particle size of aluminum from 100 to 70 nm results in an increasing particle weight gain during the surface oxidation stage from 5 to 13%, respectively. Nevertheless, decreasing the aluminum particle size to 40 nm gives about ~11% lower particle weight gain than that of Al 70 nm. It can be depicted that the lower proportion of particle weight gain of Al 40 nm compared to Al 70 nm correlates with the agglomeration of Al 40 nm particles as stated earlier (see Table 2).

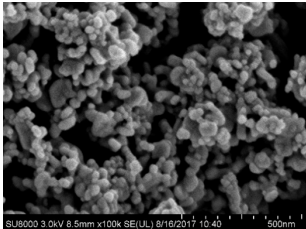
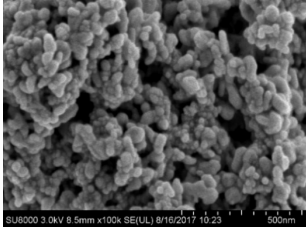
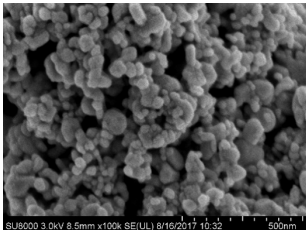
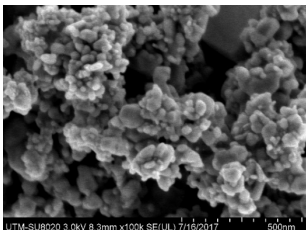
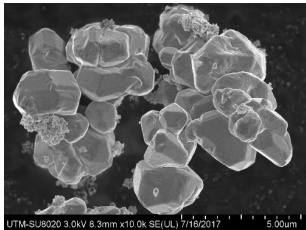
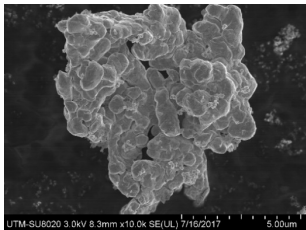
In contrast to aluminum powder, the TG curves of silver powder in Figure 6 show a very small percentage in particle weight gain, and this condition could imply that silver experiences quite a sluggish oxidation process. A similar result of the TG curve of silver powder was presented in the literature.<sup>16</sup> It is depicted that this result corresponds to the smaller specific surface area of silver powder compared to aluminum powder shown in the BET analysis. Due to this

sluggish oxidation reaction of silver, and how the aluminum oxidation reaction provides a clear indication on the explosion severity on both metal powders, it would be interesting to determine the changes in the explosion severity if the silver powder, in proportion, is added to aluminum, which will be detailed in Part II of this paper for later publication.

**3.4. Explosion Product Analysis and Kinetic Mechanism of the Single Aluminum and Silver Powder Explosion.** To further justify that silver experienced slower oxidation, the chemical composition of the explosion products of aluminum and silver powder was analyzed using X-ray photoelectron spectroscopy (XPS) analysis. The results from this analysis will be used in proposing the kinetic mechanism of the aluminum and silver powder explosion. The survey spectra of explosion products of aluminum and silver are demonstrated in Figure 7, and the corresponding binding energy values are presented in Table 4. It should be noted that all three sizes of both metal powders have similar survey spectra. For the brevity and clarity in this segment, only survey spectra of Al 70 nm and Ag 20 nm are presented. In the survey spectrum of 70 nm aluminum explosion products, we can observe aluminum 2p spectra (Al 2p) photoelectron peaks at a binding energy of 73.6 eV and oxygen 1s spectra (O 1s) at a binding energy of 530.6 eV. Meanwhile, in the survey spectrum of 20 nm silver explosion products, we can observe the silver 3d spectra (Ag 3d) photoelectron peaks at a binding energy of 366 eV and O 1s at a binding energy of 529 eV.

By resolving the high-resolution spectra of 70 nm aluminum, it was found that aluminum explosion products only comprise

Table 3. Morphological Structures of Various Sizes of Silver Particles

	Pre-explosion	Post-explosion
Ag 20 nm		
Ag 100 nm		
Ag 10 μm		

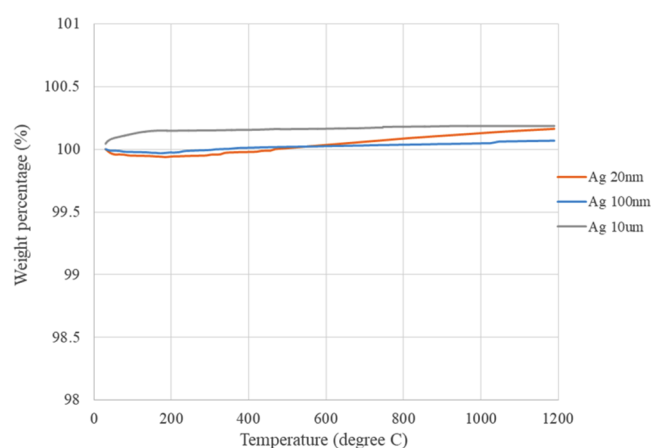


Figure 5. Oxidation process of aluminum particles based on TG curves.

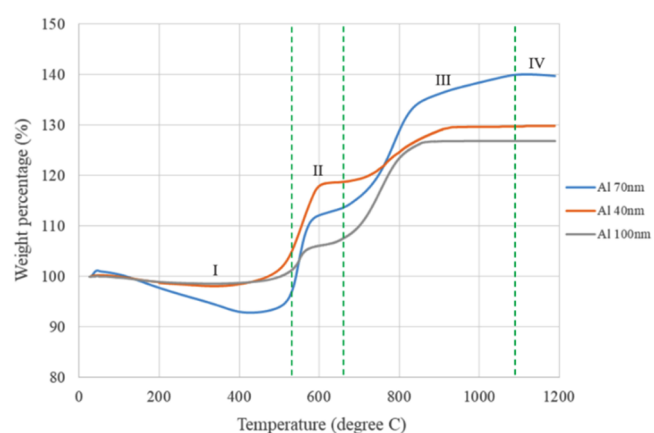
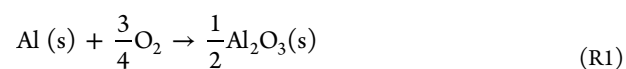


Figure 6. Oxidation process of silver particles based on TG curves.

$\text{Al}_2\text{O}_3$  at the binding energy  $E_b$  (Al 2p) of 73.6 eV. This finding is consistent with the work by Gao et al. (2017), implying that the aluminum explosion was completed in the gas-phase reaction as shown in the TGA result (see Figure 5). The resolved XPS spectrum of aluminum powder is presented in Figure 8a. Meanwhile, the resolved Ag 3d spectrum of silver powder explosion, as shown in Figure 8b, was composed of two peaks situated at binding energies of 367.92 and 373.9 eV, which corresponded to the binding energy of Ag and  $\text{Ag}_2\text{O}$ .

Based on this explosion product analysis, it is inferred that the explosion reaction of aluminum and silver powder was as in R1 R1 and R2–R3, respectively. From the product composition of 59.9% of Ag and 40.1% of  $\text{Ag}_2\text{O}$ , it can be said that the dominant reaction for silver is



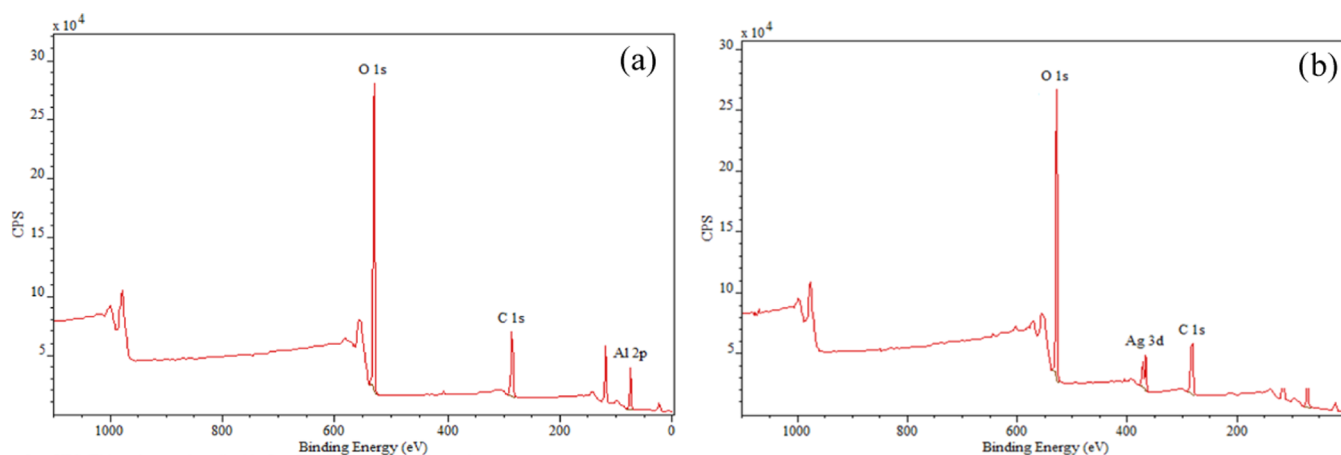


Figure 7. Survey spectra of explosion products of (a) Al 70 nm and (b) Ag 20 nm.

Table 4. Binding Energies of Survey Spectra of Al 70 nm and Ag 20 nm Explosion Products

explosion products	$E_b$ (Al 2p)/eV	$E_b$ (Ag 3d)/eV	$E_b$ (C 1s)/eV	$E_b$ (O 1s)/eV
Al 70 nm	73.6		284.6	530.6
Ag 20 nm		366.0	284.6	529.0

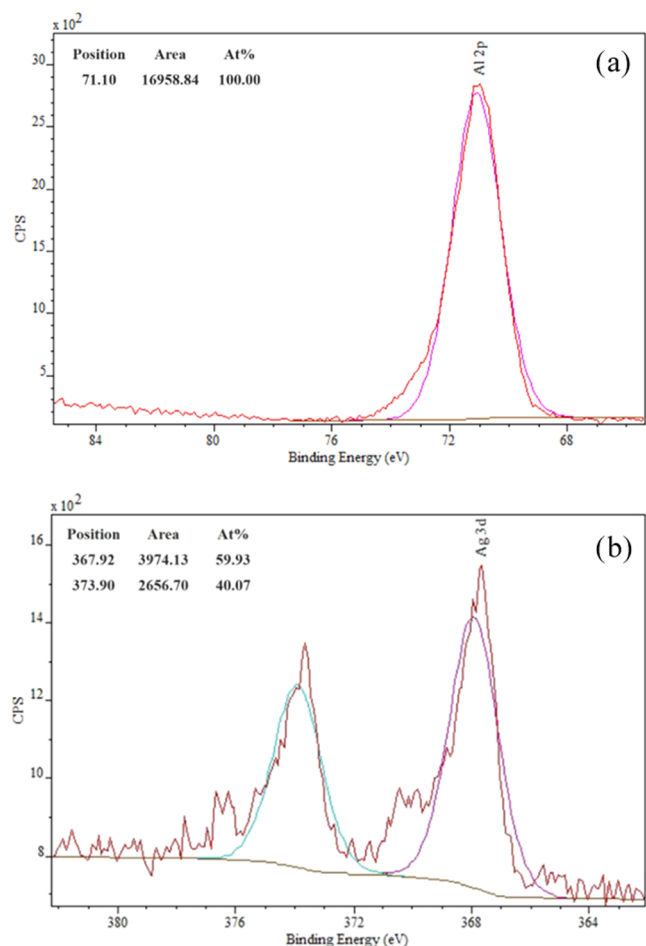
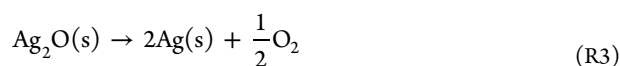


Figure 8. XPS spectra of (a) Al 2p region of Al 70 nm and (b) Ag 3d region of Ag 20 nm explosion product.



## 4. CONCLUSIONS

The present work explored the explosion characteristics of pure aluminum and silver powder. It was demonstrated that the  $P_{\max}$  and  $dP/dt_{\max}$  values of metal powder increase with decreasing particle size. However, the agglomeration effect in smaller particles reduced the specific surface area for the oxidation reaction, reflecting the reduction of particle weight gain in the thermogravimetric (TG) curve of the metal powder. The particles' agglomeration, which is more apparent in silver compared to aluminum powder, elucidates the sluggish oxidation reaction of silver powder, as illustrated in the TG curve, and hence justifies the lower  $P_{\max}$  and  $dP/dt_{\max}$  values of silver than that of aluminum powder. These findings, which provided a clear indication of the explosion severity on both metal powders, will be a basis for the future work in determining the changes in the explosion severity if the silver powder, in proportion, is added to the aluminum explosion.

## AUTHOR INFORMATION

### Corresponding Author

Rafiziana Md Kasmani – Department of Energy Engineering, School of Chemical and Energy Engineering, Universiti Teknologi Malaysia, 81310 Johor, Malaysia; [orcid.org/0000-0001-6240-296X](https://orcid.org/0000-0001-6240-296X); Phone: +6075535549; Email: rafiziana@utm.my

### Authors

Khairiah Mohd Mokhtar – Department of Chemical Engineering, Faculty of Engineering, Universiti Malaya, 50603 Kuala Lumpur, Malaysia

Che Rosmani Che Hassan – Department of Chemical Engineering, Faculty of Engineering, Universiti Malaya, 50603 Kuala Lumpur, Malaysia

Mahar Diana Hamid – Department of Chemical Engineering, Faculty of Engineering, Universiti Malaya, 50603 Kuala Lumpur, Malaysia

Mohamad Iskandr Mohamad Nor – Department of Chemical Engineering, Faculty of Engineering, Universiti Malaya, 50603 Kuala Lumpur, Malaysia

Mohd Usman Mohd Junaidi – Department of Chemical Engineering, Faculty of Engineering, Universiti Malaya, 50603 Kuala Lumpur, Malaysia; [orcid.org/0000-0003-0347-2495](https://orcid.org/0000-0003-0347-2495)

Norazana Ibrahim – Department of Energy Engineering,  
School of Chemical and Energy Engineering, Universiti  
Teknologi Malaysia, 81310 Johor, Malaysia

Complete contact information is available at:  
<https://pubs.acs.org/10.1021/acsoomega.1c00967>

### Author Contributions

K.M.M. carried out the experiment, analysis, and manuscript drafting. R.M.K. took the lead in manuscript writing, with support from C.R.C.H. and M.D.H. M.I.M.N., M.U.M.J., and N.I. contributed to the interpretation of the results. All authors provided critical feedback and helped shape the research, analysis, and manuscript.

### Funding

This research was funded by Ministry of Higher Education Malaysia (MOHE) under the Fundamental Research Grant Scheme (FRGS) [Grant no : R.J130000.7851.5F392], University of Malaya [Grant No: GPF065A-2018] and Universiti Teknologi Malaysia [Grant No : UTM CRG Q.J130000.2451.08G95/R.J130000.7351.4B572 ].

### Notes

The authors declare no competing financial interest.

## REFERENCES

- (1) Taveau, J.; Hochgreb, S.; Lemkowitz, S.; Roekaerts, D. Explosion hazards of aluminum finishing operations. *J. Loss Prev. Process Ind.* **2018**, *51*, 84–93.
- (2) Zhang, J.; Chen, H.; Liu, Y.; Elledge, H.; Mashuga, C. V.; Mannan, M. S. Explosion hazards of aluminum finishing operations. *Ind. Eng. Chem. Res.* **2015**, *54*, 3989–3995.
- (3) Wang, Q.; Sun, Y.; Zhang, Z.; Shu, C. M. Ignition and explosion characteristics of micron-scale aluminum–silicon alloy powder. *J. Loss Prev. Process Ind.* **2019**, *62*, No. 103940.
- (4) D'amico, M.; Dufaud, O.; Latché, J. C.; Trélat, S.; Perrin, L. Parametric study of the explosivity of graphite-metals mixtures. *J. Loss Prev. Process Ind.* **2016**, *43*, 714–720.
- (5) Cao, W.; Qin, Q.; Cao, W.; Lan, Y.; Chen, T.; Xu, S.; Cao, X. Experimental and numerical studies on the explosion severities of coal dust/air mixtures in a 20-L spherical vessel. *Powder Technol.* **2017**, *310*, 17–23.
- (6) Dufaud, O.; Traoré, M.; Perrin, L.; Chazelet, S.; Thomas, D. Experimental investigation and modelling of aluminum dusts explosions in the 20 L sphere. *J. Loss Prev. Process Ind.* **2010**, *23*, 226–236.
- (7) Mishra, D. P.; Azam, S. Experimental investigation on effects of particle size, dust concentration and dust-dispersion-air pressure on minimum ignition temperature and combustion process of coal dust clouds in a G-G furnace. *Fuel* **2018**, *227*, 424–433.
- (8) Cashdollar, K. L. Overview of dust explosibility characteristics. *J. Loss Prev. Process Ind.* **2000**, *13*, 183–199.
- (9) Eckhoff, R. K. Does the dust explosion risk increase when moving from  $\mu\text{m}$ -particle powders to powders of nm-particles? *J. Loss Prev. Process Ind.* **2012**, *25*, 448–459.
- (10) Huang, Y.; Risha, G. A.; Yang, V.; Yetter, R. A. Effect of particle size on combustion of aluminum particle dust in air. *Combust. Flame* **2009**, *156*, 5–13.
- (11) Gao, W.; Zhang, X.; Zhang, D.; Peng, Q.; Zhang, Q.; Dobashi. Flame propagation behaviours in nano-metal dust explosions. *Powder Technol.* **2017**, *321*, 154–162.
- (12) Sun, J.; Dobashi, R.; Hirano, T. Structure of flames propagating through aluminum particles cloud and combustion process of particles. *J. Loss Prev. Process Ind.* **2006**, *19*, 769–773.
- (13) Bouillard, J.; Vignes, A.; Dufaud, O.; Perrin, L.; Thomas, D. Ignition and explosion risks of nanopowders. *J. Hazard. Mater.* **2010**, *181*, 873–880.

(14) Mittal, M. Explosion characteristics of micron-and nano-size magnesium powders. *J. Loss Prev. Process Ind.* **2014**, *27*, 55–64.

(15) Li, Q.; Zhang, G.; Zheng, Y.; Liu, J.; Li, X. Investigation on the correlations between thermal behaviors and explosion severity of aluminum dust/air mixtures. *Powder Technol.* **2019**, *355*, 582–592.

(16) Fergus, J. W.; Mallipedi, C. V.; Edwards, D. L. Silver/silver-oxide composite coating for intrinsically adaptive thermal regulation. *Composites, Part B* **1998**, *29*, 51–56.